Scientific Research Publishing

Journal of Power and Energy Engineering, 2026, 14(11), 30-51
https://www.scirp.org/journal/jpee
ISSN Online: 2327-5901
ISSN Print: 2327-588X

Voltage Stability and Power Flow Assessment of Industrial Load Integration under 12 MW PV Injection in Congo's Grid

Rodolphe Gomba[1*], Haroun Abba Labane[2], Tite Lawd Ngouloubi[1], Eyandzi Amos Omboua[1], Ursula Vanelie Kani Mboyo[1]

[1]Laboratory of Electrical Engineering and Electronics, Polytechnic Superior National School (ENSP), Marien Ngouabi University, Brazzaville, Congo
[2]Laboratory of Electrical Engineering and Electronics, Polytechnic University of Mongo, Mongo, Chad
Email: *gombarodolphe@gmail.com, ombouaweb@gmail.com

How to cite this paper: Gomba, R., Labane, H.A., Ngouloubi, T.L., Omboua, E.A. and Kani Mboyo, U.V. (2026) Voltage Stability and Power Flow Assessment of Industrial Load Integration under 12 MW PV Injection in Congo's Grid. *Journal of Power and Energy Engineering*, **14**, 30-51.
https://doi.org/10.4236/jpee.2026.1411003

Received: September 23, 2026
Accepted: November 6, 2026
Published: November 9, 2026

Copyright © 2026 by author(s) and Scientific Research Publishing Inc.
This work is licensed under the Creative Commons Attribution International License (CC BY 4.0).
http://creativecommons.org/licenses/by/4.0/

Open Access

Abstract

The integration of utility-scale photovoltaic generation into weak power systems can significantly affect power-flow distribution and voltage-stability margins, particularly when supplying reactive industrial loads. This paper investigates a **12 MW grid-connected photovoltaic plant supplying a 22 MVA industrial load** under weak-grid conditions. The proposed assessment combines Newton-Raphson power flow, continuation-based P-V analysis, Jacobian minimum singular-value monitoring, and static var generator (SVG) compensation. For the adopted reduced benchmark with a short-circuit ratio of SCR = 5, the uncompensated system exhibits severe voltage degradation and limited loadability. A **6 MVAr SVG** increases the minimum bus voltage from 0.617 to 0.855 p.u. and the maximum loading factor from 0.023 to 0.316. The corresponding maximum industrial active load increases from 19.13 to 24.61 MW, while active-power losses decrease from 0.924 to 0.210 MW. However, the compensated voltage remains below the 0.95 p.u. criterion, indicating that nominal reactive-power compensation alone does not ensure adequate voltage performance in a weak grid. The results highlight the need for **SVG sizing based jointly on voltage regulation and static loadability constraints**. Here, λ is the fractional load increase, with $\lambda = 0$ at nominal demand. The reported results require verification using the complete network dataset and actual SVG control settings.

Keywords

Photovoltaic Integration, Voltage Stability, Power Flow, Industrial Load, Weak Grid, Static Var Generator, Continuation Power Flow, Reactive-Power Compensation

1. Introduction

Large-scale photovoltaic integration modifies active-reactive power flows and voltage regulation, particularly in weak grids supplying industrial loads. Low short-circuit strength and high reactive-power demand can produce significant voltage deviations and reduce the static loadability margin [1]-[3]. This issue is relevant to the **Republic of the Congo**, where renewable generation and transmission-system reinforcement are being pursued. The integration of utility-scale PV therefore requires assessment of both power-flow feasibility and voltage-stability constraints. For industrial loads, active-power balance alone is insufficient. Reactive-power transfer, grid strength, and network impedance directly affect bus voltages and proximity to voltage instability [4] [5]. Moreover, increasing inverter-based generation can reduce available reactive-power reserves, making voltage stability increasingly dependent on local reactive support and network strength [6]. Recent studies confirm that renewable penetration and reactive-power availability must be jointly considered when evaluating voltage-stability margins [7]. SVG/STATCOM compensation can provide local reactive support [8] [9]; however, a rating derived solely from nominal reactive demand does not necessarily guarantee an acceptable voltage-stability margin. Under weak-grid conditions, the compensator rating must therefore be assessed against both the required voltage range and maximum transferable load [10]. This paper investigates a **12 MW grid-connected PV plant supplying a 22 MVA industrial load** under weak-grid conditions. Newton-Raphson power flow, continuation-based P-V analysis, the minimum singular value of the power-flow Jacobian, and SVG compensation are jointly applied [11]-[13]. The main contributions are:

- A unified **PV-grid-PCC-industrial load-SVG** power-flow model;
- Critical-bus and loadability-limit identification using P-V continuation and $\sigma\min(J)$;
- Quantitative assessment through Vmin, network losses, λmax, and PL, max;
- Evaluation of SVG sizing under simultaneous **voltage-regulation and loadability constraints**.

2. Technical Background and Research Gap

2.1. PV Integration and Weak-Grid Voltage Stability

High PV penetration modifies active-reactive power exchanges and increases voltage sensitivity when grid short-circuit strength is limited [1]-[5]. For inverter-based generation, voltage stability is strongly influenced by grid impedance, reactive-power capability, and load characteristics. Static voltage stability is assessed from P-V trajectories and the maximum loading point. Near the stability boundary,

$$\lambda \to \lambda_{\max}, \sigma_{\min}(J) \to 0$$

where J denotes the power-flow Jacobian [11]-[13]. Recent continuation-power-flow developments extend this assessment to networks containing distributed and

inverter-based resources [14]. The 2025 IEEE work associated with [14], for example, develops an integrated CPF formulation accounting for DERs, load types, network imbalance and renewable fluctuations.

These indicators are subsequently adopted for the investigated PV-industrial system.

2.2. Reactive-Power Support

Reactive-power availability directly affects voltage regulation in weak networks [6] [7]. SVG/STATCOM devices provide controllable reactive support at critical buses and can modify both the voltage profile and system loadability [8]-[10].

The compensation requirement cannot therefore be reduced to nominal reactive-power balance. Under weak-grid conditions, the SVG rating must additionally satisfy

$$V_{\min} \geq V_{\lim}$$

while maintaining an adequate static loading margin.

The preliminary compensation rating must therefore be evaluated against both voltage performance and the static loadability boundary, rather than nominal power-factor correction alone.

2.3. Research Gap

Existing studies address weak-grid strength, renewable penetration, continuation-based voltage-stability assessment, and reactive-power compensation [1]-[15]. However, the engineering problem considered here requires these quantities to be evaluated within the same operating framework.

Accordingly, this study considers

$$\text{12 MW PV} \rightarrow \text{Weak Grid/PCC} \rightarrow \text{22 MVA Industrial Load} \rightarrow \text{SVG}$$

and evaluates the compensation requirement simultaneously against bus-voltage, network-loss, and static-loadability constraints.

3. Overall System Architecture

High PV penetration affects power-flow distribution and voltage regulation, particularly in weak grids, where adequate reactive-power support becomes critical for maintaining acceptable voltage conditions.

The investigated system consists of a 12 MW grid-connected PV plant, an upstream utility grid, a point of common coupling (PCC), transformation and transmission interfaces, industrial loads, and a reactive-power compensation unit, as illustrated in **Figure 1**. The PCC constitutes the main electrical interface for assessing active- and reactive-power exchanges between the PV plant, utility grid, and industrial network.

The PV plant operates at a rated active power of

$$P_{PV,rated} = 12MW \tag{1}$$

The industrial subsystem comprises aggregated loads connected downstream

of the PCC. Since industrial loading may impose significant reactive-power requirements, the compensation device is located at the critical bus identified from the uncompensated power-flow and voltage-stability analyses rather than being predefined.

The system assessment is based on the electrical quantities

$$M = \left\{ V_i, P_{ij}, Q_{ij}, P_{loss}, Q_{loss} \right\} \tag{2}$$

where V_i denotes the voltage magnitude at bus i, P_{ij} and Q_{ij} are the active and reactive power transfers between buses i and j, and P_{loss} and Q_{loss} represent the network active- and reactive-power losses. The critical bus and voltage-stability margins are subsequently determined using the assessment methodology developed in Section 5.

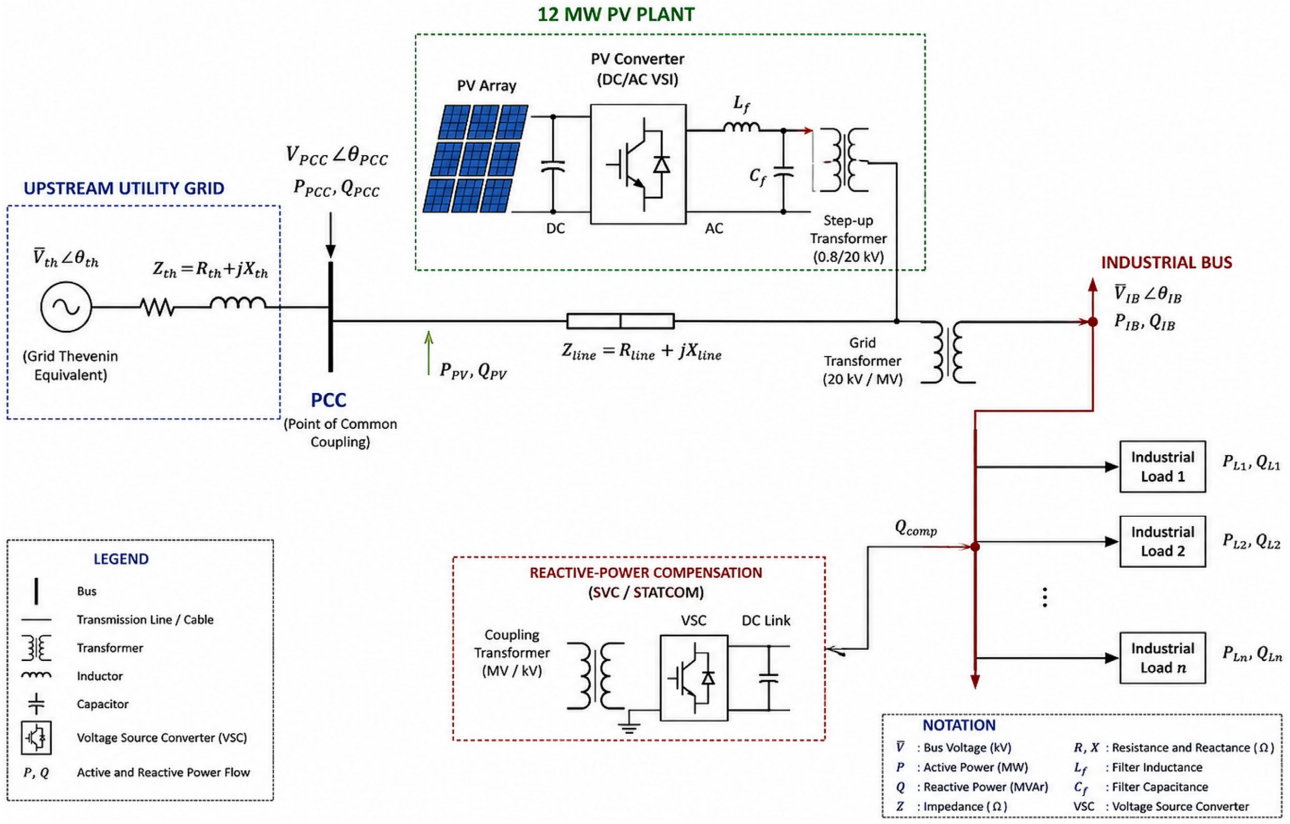


Figure 1. Conceptual single-line architecture with reactive compensation at the industrial bus. This equipment diagram does not replace the numerical solver bus and branch dataset.

3.1. Grid and Network Specifications

The upstream network is represented by a 220 kV transmission grid interconnected with the 12 MW PV-industrial system through the PCC. The Congolese transmission network includes 220 kV and 110 kV backbone levels, with 30 - 35 kV subtransmission interfaces. For the investigated configuration, the upstream source is represented at 220 kV, while a 20 kV PCC is adopted for the PV and industrial subsystems.

The nominal system frequency is fixed at

$$f_n = 50 \text{ Hz} \tag{3}$$

To investigate a moderately weak operating condition, the base-case short-circuit ratio is set to

$$SCR = 5 \tag{4}$$

With a 12 MW PV rated power, the corresponding short-circuit capacity adopted at the PCC is

$$S_{sc} = SCR\, P_{PV,rated} = 5 \times 12 = 60 MVA \tag{5}$$

An X/R ratio of 10 is adopted for the equivalent upstream impedance. The values $SCR = 5$ and $X/R = 10$ are treated as simulation assumptions rather than measured parameters of the Congolese transmission system. Their influence can subsequently be examined through sensitivity analysis, as shown in Table 1.

Table 1. Electrical specifications of the studied grid.

Parameter	Symbol	Value	Unit	Status
Upstream transmission voltage	V_G	220	kV	Congo grid
PCC voltage	V_{PCC}	20	kV	Study configuration
Nominal frequency	f_n	50	Hz	Congo grid
PV rated power	$P_{PV,\text{rated}}$	12	MW	Case study
Base power	S_{base}	100	MVA	Simulation base
Base PCC voltage	V_{base}	20	kV	Simulation base
Short-circuit ratio	SCR	5	—	Adopted
Short-circuit capacity	S_{sc}	60	MVA	Calculated
Grid X/R ratio	X/R	10	—	Adopted
PV transformer	T_{PV}	0.8/20	kV/kV	Study configuration
Grid transformer	T_G	220/20	kV/kV	Study configuration

The 220/20 kV and 0.8/20 kV transformer ratios define the adopted study configuration; they are not presented as measured ratings of a specific 12 MW Congolese PV installation. Detailed equivalent impedances, per-unit conversion, network admittances, and power-flow equations are developed separately in Section 4.

Reproducibility requires a numerical bus and branch dataset in addition to the conceptual architecture. The voltage-profile figures distinguish the upstream source, PCC, and industrial bus; they do not specify the complete solver connectivity. The 220/20 kV and 0.8/20 kV transformer ratios alone do not determine leakage impedance, tap position, or transformer losses. The PCC Thévenin impedance derived in Section 5.2 is an aggregate upstream equivalent: if it already includes the grid transformer, that impedance must not be counted again as a separate series element. The PV plant is represented by fixed P and Q injections, not by a voltage-controlled PV bus merely because the generator is photovoltaic.

3.2. 12 MW Photovoltaic Plant Specifications

The photovoltaic plant is represented as a utility-scale generation unit with a rated AC active-power capacity of

$$P_{PV,rated} = 12MW \tag{6}$$

The conversion chain comprises the PV array, DC-link stage, grid-connected voltage-source converter (VSC), output filter, and step-up transformer interfacing the plant with the 20 kV PCC. For system-level power-flow analysis, the internal switching dynamics are neglected and the PV plant is represented at its AC terminal by its active- and reactive-power operating setpoints.

Under nominal irradiance and temperature conditions, the available active power is bounded by

$$0 \le P_{PV} \le P_{PV,rated} \tag{7}$$

The inverter apparent-power capability imposes the operating constraint

$$P_{PV}{}^2 + Q_{PV}{}^2 \le S_{inv}{}^2 \tag{8}$$

which defines the reactive-power capability available for voltage support at a given active-power operating point. Consequently, the maximum inverter reactive-power magnitude is

$$\left|Q_{PV}\right| \le \sqrt{S_{inv}{}^2 - P_{PV}{}^2} \tag{9}$$

For the base operating condition, the PV plant is operated at unity power factor,

$$P_{PV} = 12MW, Q_{PV} = 0 \tag{10}$$

thereby allowing the effect of the external reactive-power compensation system to be evaluated independently. Additional operating cases may subsequently exploit the inverter reactive-power capability to assess coordinated voltage support, as shown in Table 2.

Table 2. Main specifications of the 12 MW PV plant.

Parameter	Symbol	Value	Unit	Status
Rated AC active power	$P_{PV,\text{rated}}$	12	MW	Case study
PCC voltage	V_{PCC}	20	kV	Study configuration
Nominal frequency	f_n	50	Hz	System
Converter topology	—	VSC	—	Adopted
Converter AC voltage	V_{inv}	0.8	kV	Study configuration
Step-up transformer	T_{PV}	0.8/20	kV/kV	Study configuration
Base-case active power	P_{PV}	12	MW	Operating point
Base-case reactive power	Q_{PV}	0	MVAr	Adopted
Base-case power factor	pf_{PV}	1.0	—	Adopted
Nominal irradiance	G_{ref}	1000	W/m^2	Reference condition
Reference temperature	T_{ref}	25	˚C	Reference condition

The inverter apparent-power rating S_{inv} is intentionally left unspecified until a documented converter rating or a clearly justified study value is selected. This prevents an arbitrary reactive-power capability from influencing the subsequent voltage-stability assessment.

3.3. Industrial Load Specifications

The industrial subsystem is represented by aggregated three-phase loads connected downstream of the 20 kV PCC. A nominal apparent-power demand of

$$S_{L0} = 22MVA \tag{11}$$

is adopted as the reference operating condition. The load is considered predominantly inductive, with a reference lagging power factor of

$$pf_{L0} = 0.85 \tag{12}$$

Accordingly, the nominal active-power demand is

$$P_{L0} = S_{L0} pf_{L0} = 22 \times 0.85 = 18.70MW \tag{13}$$

while the corresponding reactive-power demand is

$$Q_{L0} = S_{L0} \sqrt{\left(1 - pf_{L0}^{\ 2}\right)} = 22\sqrt{\left(1 - 0.85^2\right)} = 11.59MVAr \tag{14}$$

The reference industrial operating point is therefore

$$S_{L0} = P_{L0} + jQ_{L0} = 18.70 + j11.59MVA \tag{15}$$

The loading parameter λ denotes the fractional increase relative to the nominal 22 MVA demand: $S_L(\lambda) = (1 + \lambda)S_{L0}$. Thus $\lambda = 0$ is nominal, $\lambda = -0.50$ is half load, and $\lambda = 0.50$ is 150% of nominal load. Table 3 uses this same convention as Equation (56) and the P-V figures. The total load multiplier is $\alpha = 1 + \lambda$; α and λ must not be interchanged. The listed load levels are screening cases, not evidence of feasible power-flow solutions; feasibility is checked separately for each compensation case as shown in Table 3.

Table 3. Industrial load operating conditions.

Operating condition	$\lambda = S_L/S_{L0} - 1$	P_L (MW)	Q_L (MVAr)	S_L (MVA)	pf_L
Light	−0.50	9.35	5.80	11.00	0.85
Moderate	−0.25	14.03	8.69	16.50	0.85
Nominal	0.00	18.70	11.59	22.00	0.85
High	0.25	23.38	14.49	27.50	0.85
Severe	0.50	28.05	17.39	33.00	0.85

At the nominal operating point, the ratio between the rated PV generation and industrial active-power demand is

$$K_{PV} = \frac{P_{PV,rated}}{P_{L0}} = \frac{12}{18.70} = 0.642 \tag{16}$$

Thus, the rated PV generation corresponds to approximately 64.2% of the nominal industrial active-power demand. Neglecting network losses, the remaining active-power requirement at rated PV production is approximately

$$P_G \approx 18.70 - 12 = 6.70MW$$

This operating condition maintains simultaneous participation of the PV plant and the upstream utility grid, providing a consistent reference state for the subsequent power-flow and voltage-stability assessments.

The equations used here represent the aggregated industrial demand as a balanced, constant-power PQ load: at any fixed λ, P_L and Q_L do not depend on bus voltage. This is an assumption of the static model, not an identified composition of the actual industrial process. No induction-motor dynamics, stalling, protection action, or load recovery is represented. A ZIP sensitivity study should distinguish constant-power, constant-current, and constant-impedance contributions. At depressed voltage, current and impedance components reduce demand relative to the constant-power case; their effect on the fold must be recalculated rather than assigned a universal numerical correction. Static loadability does not establish motor ride-through or dynamic voltage stability.

3.4. Reactive Power Compensation System

A 6 MVAr shunt-connected SVG is considered at the critical industrial bus, downstream of the PCC. This location is used consistently in **Figure 1** and **Figure 2** and Sections 4.5 and 6.3. It provides local reactive-power support in the static power-flow model; dynamic converter performance is outside the present assessment.

For the nominal industrial load,

$$P_{L0} = 18.70MW, Q_{L0} = 11.59MVAr, pf_{L0} = 0.85 \tag{17}$$

The preliminary reactive-power requirement is determined for a target power factor $pf_t = 0.95$ as

$$Q_{comp} = P_{L0}\left[\tan\left(\cos^{-1} pf_{L0}\right) - \tan\left(\cos^{-1} pf_t\right)\right] \tag{18}$$

Substituting the nominal operating conditions gives

$$Q_{comp} = 18.70\left[\tan\left(\cos^{-1} 0.85\right) - \tan\left(\cos^{-1} 0.95\right)\right] = 5.44MVAr \tag{19}$$

Accordingly, the initial SVG rating is selected as

$$Q_{SVG,rated} = 6MVAr \tag{20}$$

at the 20 kV industrial bus. The SVG operating range is defined by

$$-6 \le Q_{SVG} \le 6MVAr \tag{21}$$

Positive Q_{SVG} denotes capacitive injection and negative Q_{SVG} denotes inductive absorption. The ±6 MVAr rating is a capability bound, not the actual injection. Actual nominal and critical injections must be exported from the converged solutions. The target power factor of 0.95 used for preliminary sizing is distinct from the SVG voltage reference (**Table 4**).

Table 4. SVG specifications.

Parameter	Symbol	Value	Unit
Connection voltage	V_{SVG}	20	kV
Initial load power factor	pf_{I0}	0.85	—
Target power factor	pf_t	0.95	—
Calculated compensation	Q_{comp}	5.44	MVAr
Rated SVG capacity	$Q_{SVG,\text{rated}}$	6	MVAr
Reactive-power range	Q_{SVG}	−6 to +6	MVAr
Connection type	—	Shunt	—
Control variable	—	Bus voltage	—
Connection bus	k	Industrial bus downstream of PCC	—
Voltage reference	V_{ref}	AUTHOR TO CONFIRM	p.u.
Voltage droop	K_Q	AUTHOR TO CONFIRM	p.u./MVAr
Actual injection at nominal load	$Q_{SVG}(0)$	EXPORT REQUIRED	MVAr
Actual injection at critical load	$Q_{SVG}(\lambda_{\max})$	EXPORT REQUIRED	MVAr

4. Mathematical Modeling and Power-Flow Formulation

4.1. Network Admittance Formulation

For an N-bus balanced three-phase AC network, the nodal equations are obtained from Kirchhoff's current law at each bus i:

$$I_i = \sum_{j\in\Omega_i} I_{ij} + I_i^{sh}, i = 1,\cdots,N \tag{22}$$

where Ω_i denotes the set of buses directly connected to bus i, I_{ij} is the current flowing from bus i to bus j, and I_i^{sh} represents the total shunt current connected to bus i.

For a transmission branch (i, j), the series impedance is

$$Z_{ij} = R_{ij} + jX_{ij} \tag{23}$$

and the associated series admittance is

$$y_{ij} = \frac{1}{Z_{ij}} = \frac{R_{ij} - jX_{ij}}{R_{ij}^2 + X_{ij}^2} = g_{ij} + jb_{ij} \tag{24}$$

with

$$g_{ij} = \frac{R_{ij}}{R_{ij}^2 + X_{ij}^2}, b_{ij} = -\frac{X_{ij}}{R_{ij}^2 + X_{ij}^2} \tag{25}$$

Using the conventional π-equivalent model, the total line-charging susceptance B_{ij}^c is equally divided between the two terminal buses. The branch currents are therefore

$$I_{ij} = \left(y_{ij} + j\frac{B_{ij}^c}{2}\right)V_i - y_{ij}V_j \tag{26}$$

$$I_{ji} = \left(y_{ij} + j\frac{B_{ij}^{c}}{2} \right) V_j - y_{ij} V_i \tag{27}$$

Substituting the branch-current expression into Kirchhoff's current law gives

$$I_i = \sum_{j \in \Omega_i} \left[\left(y_{ij} + j\frac{B_{ij}^{c}}{2} \right) V_i - y_{ij} V_j \right] + y_i^{sh} V_i \tag{28}$$

Rearranging the voltage-dependent terms yields

$$I_i = \left[\sum_{j \in \Omega_i} \left(y_{ij} + j\frac{B_{ij}^{c}}{2} \right) + y_i^{sh} \right] V_i - \sum_{j \in \Omega_i} y_{ij} V_j \tag{29}$$

Hence, the injected current at bus i can be expressed as

$$I_i = \sum_{j=1}^{N} Y_{ij} V_j \tag{30}$$

The off-diagonal elements of the bus-admittance matrix are given by

$$Y_{ij} = -y_{ij}, i \neq j \tag{31}$$

while each diagonal element is obtained from the sum of all series and shunt admittances incident on bus i:

$$Y_{ii} = y_i^{sh} + \sum_{j \in \Omega_i} \left(y_{ij} + j\frac{B_{ij}^{c}}{2} \right) \tag{32}$$

The complete nodal relationship is therefore written as

$$I = Y_{bus} V \tag{33}$$

$$I = \left[I_1, I_2, \cdots, I_N \right]^T, V = \left[V_1, V_2, \cdots, V_N \right]^T \tag{34}$$

$$Y_{bus} = \left[Y_{ij} \right]_{N \times N} \tag{35}$$

Because the studied system includes both the 220/20 kV grid transformer and the 0.8/20 kV PV step-up transformer, off-nominal transformer ratios are explicitly incorporated into the nodal admittance formulation. For a transformer connected between buses i and j, the complex tap ratio is defined as

$$a_{ij} = \tau_{ij} e^{j\theta_{ij}} \tag{36}$$

where τ_{ij} denotes the tap magnitude and θ_{ij} the phase-shifting angle. The corresponding transformer series admittance is

$$y_{ij}^{T} = \frac{1}{R_{ij}^{T} + jX_{ij}^{T}} \tag{37}$$

and the transformer terminal-current relationship becomes

$$\begin{bmatrix} I_i \\ I_j \end{bmatrix} = \begin{bmatrix} \dfrac{y_{ij}^{T}}{\left| a_{ij} \right|^2} & -\dfrac{y_{ij}^{T}}{a_{ij}^{*}} \\ -\dfrac{y_{ij}^{T}}{a_{ij}} & y_{ij}^{T} \end{bmatrix} \begin{bmatrix} V_i \\ V_j \end{bmatrix} \tag{38}$$

For transformers without phase shifting, $\theta_{ij} = 0$, and the complex tap ratio reduces to

$$a_{ij} = \tau_{ij} \tag{39}$$

The transformer contribution can then be written compactly as

$$Y^{T}{}_{ij} = y^{T}{}_{ij} \begin{bmatrix} \frac{1}{\tau_{ij}{}^{2}} & -\frac{1}{\tau_{ij}} \\ -\frac{1}{\tau_{ij}} & 1 \end{bmatrix} \tag{40}$$

After assembling all transmission-line, transformer, and shunt elements, the complete bus-admittance matrix is obtained as

$$Y_{bus} = Y_{line} + Y_{tr} + Y_{sh} \tag{41}$$

and expressed in rectangular form as

$$Y_{bus} = G + jB, Y_{ij} = G_{ij} + jB_{ij} \tag{42}$$

The resulting Y_{bus} matrix contains the complete steady-state electrical representation of the studied network and provides the algebraic basis for the nonlinear active- and reactive-power equations developed in Section 4.2.

4.2. Active and Reactive Power Equations

Using the admittance formulation established in Section 4.1, the current and complex-power injections at bus i are

$$I_i = \sum_{j=1}^{N} Y_{ij} V_j, S_i = P_i + jQ_i = V_i I_i^{*} \tag{43}$$

Substituting the nodal current into the complex-power expression yields

$$S_i = V_i \left(\sum_{j=1}^{N} Y_{ij} V_j \right)^{*} = V_i \sum_{j=1}^{N} Y_{ij}^{*} V_j^{*} \tag{44}$$

With

$$V_i = |V_i| e^{j\delta_i}, \; Y_{ij} = G_{ij} + jB_{ij}, \; \delta_{ij} = \delta_i - \delta_j \tag{45}$$

the complex-power injection becomes

$$S_i = \sum_{j=1}^{N} |V_i||V_j| \left(G_{ij} - jB_{ij} \right) e^{j\delta_{ij}} \tag{46}$$

Using Euler's identity and separating the real and imaginary components of (46), the nonlinear active- and reactive-power equations are obtained as

$$\left\{ \begin{array}{l} P_i = \sum_{j=1}^{N} |V_i||V_j| \left[G_{ij} \cos\delta_{ij} + B_{ij} \sin\delta_{ij} \right]; \\ Q_i = \sum_{j=1}^{N} |V_i||V_j| \left[G_{ij} sin\,\delta_{ij} - B_{ij} cos\,\delta_{ij} \right] \end{array} \right\} \tag{47}$$

For the power-flow solution, the specified net injections are defined according to the adopted positive-injection convention as

$$\begin{aligned} P_i^{spec} &= P_{Gi} + P_{PV,i} - P_{Li} \\ Q_i^{spec} &= Q_{Gi} + Q_{PV,i} + Q_{SVG,i} - Q_{Li} \\ \Delta P_i &= P_i^{spec} - P_i\left(V,\delta\right) \\ \Delta Q_i &= Q_i^{spec} - Q_i\left(V,\delta\right) \end{aligned} \tag{48}$$

The steady-state operating point is obtained when the power mismatches ΔP_i . and ΔQ_i converge to zero within the prescribed numerical tolerance. The nonlinear system defined by (47) - (48) constitutes the basis of the Newton-Raphson formulation developed in Section 4.3.

4.3. Newton-Raphson Power-Flow Solution

The nonlinear system defined by (47) - (48) is solved using the Newton-Raphson method. For a network containing one slack bus, n_{PV} PV buses, and n_{PQ} PQ buses, the state vector is defined as

$$x = \left[\delta_{PV}{}^T \; \delta_{PQ}{}^T \; V_PQ^T \right]^T, \dim\left(x\right) = n_{PV} + 2n_{PQ} \tag{49}$$

where the slack-bus voltage magnitude and angle are fixed, PV-bus voltage magnitudes are specified, and PQ-bus voltage magnitudes and phase angles are unknown.

At iteration *k*, the active- and reactive-power mismatches are assembled as

$$\Delta F^{(k)} = \left[\Delta P^{(k)} \Delta Q^{(k)} \right]^T = \left[P^{spec} - P\left(x^{(k)}\right) Q^{spec} - Q\left(x^{(k)}\right) \right]^T \tag{50}$$

Linearization around the current operating point gives

$$\Delta F^{(k)} = J^{(k)} \Delta x^{(k)}, \Delta x^{(k)} = \left[\Delta \delta^{(k)T} \Delta V_PQ^{(k)T} \right]^T \tag{51}$$

where the Newton-Raphson Jacobian is

$$J = \left[H \; N; M \; L \right] = \left[\partial P/\partial \delta \;\; \partial P/\partial V \,;\; \partial Q/\partial \delta \;\; \partial Q/\partial V \right] \tag{52}$$

For $i \neq$ j, the off-diagonal Jacobian elements follow directly from (47):

$$\begin{aligned} H_{ij} &= \left|V_i\right|\left|V_j\right|\left[G_{ij} \sin\delta_{ij} - B_{ij} \cos\delta_{ij} \right] \\ N_{ij} &= \left|V_i\right|\left[G_{ij} \cos\delta_{ij} + B_{ij} \sin\delta_{ij} \right] \\ M_{ij} &= -\left|V_i\right|\left|V_j\right|\left[G_{ij} \cos\delta_{ij} + B_{ij} \sin\delta_{ij} \right] \\ L_{ij} &= \left|V_i\right|\left[G_{ij} \sin\delta_{ij} - B_{ij} \cos\delta_{ij} \right], i \neq j \end{aligned} \tag{53}$$

The corresponding diagonal elements are

$$\begin{aligned} H_{ii} &= -Q_i - B_{ii}\left|V_i\right|^2 ; N_{ii} = P_i / \left|V_i\right| + G_{ii}\left|V_i\right| \\ M_{ii} &= P_i - G_{ii}\left|V_i\right|^2 ; L_{ii} = Q_i / \left|V_i\right| - B_{ii}\left|V_i\right| \end{aligned} \tag{54}$$

Rather than explicitly forming the inverse of the Jacobian, the state correction is obtained by solving the linear system and updating the state as

$$J^{(k)} \Delta x^{(k)} = \Delta F^{(k)}, x^{(k+1)} = x^{(k)} + \Delta x^{(k)} \tag{55}$$

Iterations are terminated when the infinity norm of the mismatch vector satisfies

$$\left\|\Delta F^{(k)}\right\|\infty \le \varepsilon$$

where ε is the prescribed convergence tolerance. The converged operating point provides the bus-voltage magnitudes, phase angles, and power transfers required for the subsequent voltage-stability assessment.

4.4. Voltage-Stability Formulation

Voltage stability is assessed with $\lambda = 0$ at the nominal operating point and $\lambda > 0$ for demand increases. Only industrial demand is scaled; the PV active-power injection remains 12 MW and Q_{PV} remains zero. The slack source balances the additional demand and network losses. At each stressed load bus,

$$P_{Li}(\lambda) = P_{Li0}(1+\lambda), Q_{Li}(\lambda) = Q_{Li0}(1+\lambda) \tag{56}$$

where P_{Li0} and Q_{Li0} denote the base-case load demand. The reference power factor is preserved through

$$Q_{Li}(\lambda)/P_{Li}(\lambda) = Q_{Li0}/P_{Li0} = \tan\left(\cos^{-1} pf_{L0}\right) \tag{57}$$

The parameterized power-flow system is

$$F(x,\lambda) = \left[\Delta P(x,\lambda)\Delta Q(x,\lambda)\right]^T = 0 \tag{58}$$

The state vector x contains the unknown voltage angles and voltage magnitudes, with the SVG control variable and equation added when voltage regulation is active. Starting from a converged high-voltage solution at $\lambda = 0$, successive solutions of (58) generate the P-V trajectories. If the nominal Newton-Raphson solution is ambiguous, a lighter-load solution must first be continued to $\lambda = 0$ to establish the selected branch.

$$|V_i| = f_i(\lambda), i \in \Omega_{PQ} \tag{59}$$

At a smooth fold of the equilibrium branch, the fixed-λ power-flow Jacobian becomes singular. This condition is evaluated within the current control regime; a change caused by an SVG limit must be distinguished from a smooth fold:

$$\det\left[J(x,\lambda)\right] \to 0, \sigma_{\min}(J) \to 0 \tag{60}$$

The minimum singular value is a supporting proximity indicator, not a standalone stopping test with an unspecified threshold. The maximum loading parameter $\lambda_{\max}$ gives the incremental margin from the nominal point:

$$\Delta P_{\text{margin}} = \lambda_{\max} P_{L0}, P_{L,\max} = (1+\lambda_{\max}) P_{L0} \tag{61}$$

For the nominal industrial demand,

$$P_{L0} = 18.70 MW$$

Consequently, $\lambda_{\max} = 0.023$ represents a 2.3% demand increase and a total multiplier $\alpha_{\max} = 1.023$; $\lambda_{\max} = 0.316$ represents a 31.6% increase and $\alpha_{\max} = 1.316$. Using the reported rounded values, the corresponding active demands are 19.13 MW and 24.61 MW, with incremental margins of 0.43 MW and 5.91 MW. These are arithmetic conversions, not new simulation results.

4.5. SVG Steady-State Model

The SVG is modeled as a controllable shunt reactive-power source connected to the critical bus k, with negligible active-power exchange:

$$S_{SVG} = P_{SVG} + jQ_{SVG}, P_{SVG} \approx 0 \tag{62}$$

The reactive-power balance at the compensated bus becomes

$$\Delta Q_k = Q_{Gk} + Q_{PV,k} + Q_{SVG} - Q_{Lk} - Q_k\left(V, \delta\right) \tag{63}$$

Voltage regulation is represented by

$$\left|V_k\right| = V_k^{ref} - K_Q Q_{SVG}, K_Q > 0 \tag{64}$$

subject to the adopted SVG capability:

$$-6 \le Q_{SVG} \le +6MVAr \tag{65}$$

For positive droop K_Q, the unsaturated SVG solves Equation (64) together with the reactive-power balance; the bus is not an ideal fixed-voltage PV bus. K_Q has units of p.u./MVAr when Q_{SVG} is expressed in MVAr. With $K_Q = 0$, the unsaturated model becomes ideal voltage regulation. At +6 or −6 MVAr, reactive injection is fixed at the reached bound, the voltage-control equation is released, and the industrial-bus voltage is solved as a PQ variable. A saturated point is accepted only while the unconstrained control demand would remain beyond that bound; otherwise, voltage regulation is restored. No numerical voltage reference or droop is inferred from the nameplate rating.

[Enter the actual V_{ref} and K_Q used in the simulation, with units, and export Q_{SVG} at $\lambda = 0$ and at the critical point. The reported voltage of 0.855 p.u. does not by itself establish saturation at +6 MVAr. These values cannot be reconstructed uniquely from the present tables.]

5. Simulation Methodology and Study Cases

5.1. Simulation Framework

The developed power-flow and voltage-stability models are implemented for the 12 MW PV-industrial network using the parameters defined in Section 3. The base operating condition is

$$P_{PV} = 12MW, S_{L0} = 22MVA, pf_{L0} = 0.85 \tag{66}$$

corresponding to

$$P_{L0} = 18.70MW, Q_{L0} = 11.59MVAr \tag{67}$$

The power-flow solution is obtained using the Newton-Raphson formulation of Section 4.3. Convergence is imposed when

$$\max_i abs\left(\Delta F_i\right) \le 10^{-6} \tag{68}$$

A reproducible continuation calculation should use the predictor-corrector protocol specified below. The implementation and settings must be checked against the solver that produced the reported curves before those curves are accepted as validated results. The following two compensation configurations are eval-

uated:

$$C_{OFF} : Q_{SVG} = 0$$
$$C_{ON} : -6 \le Q_{SVG} \le +6MVAr \tag{69}$$

The technical performance vector is defined as

$$\Gamma = \left[V_{\min}, P_{\text{loss}}, Q_{\text{loss}}, \lambda_{\max}, \Delta P_{\text{margin}} \right] \tag{70}$$

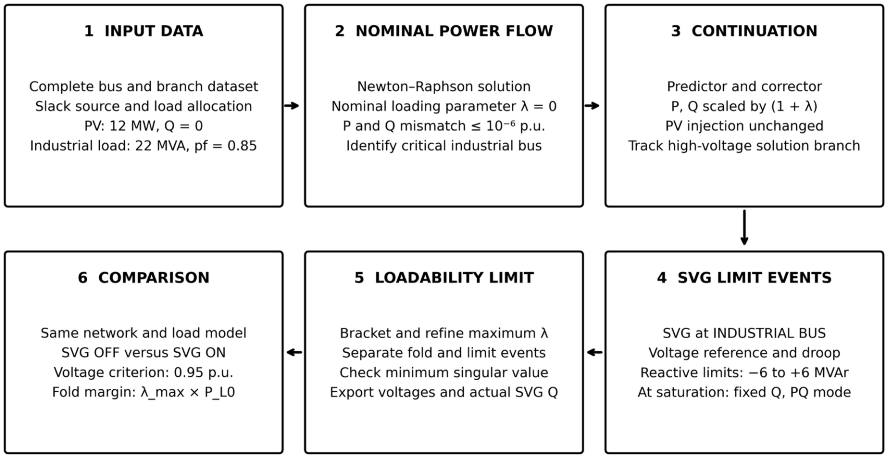


Figure 2. Revised assessment workflow with SVG at the industrial bus and $\lambda = 0$ at nominal load. Predictor-corrector and event settings require verification against the original implementation.

Table 5. Simulation cases.

Case	PV injection	Industrial load	SVG	Main objective
C0	12 MW	22 MVA	OFF	Base uncompensated power flow
C1	12 MW	Variable	OFF	Uncompensated P-V characteristic
C2	12 MW	22 MVA	6 MVAr	Compensated nominal operation
C3	12 MW	Variable	6 MVAr	Compensated P-V characteristic

The comparison between C1 and C3 quantifies the effect of reactive-power compensation on the maximum loading capability and voltage-stability margin (Table 5).

Continuation verification protocol. Use $y = (x, \lambda)$ and a normalized tangent t satisfying $[F_x\ F_\lambda]t = 0$. Predict $y_p = y_n + h \times t_n$, then correct $F(x, \lambda) = 0$ with the pseudo-arclength condition $t_{n^T}\ (y - y_p) = 0$. Choose the tangent orientation continuously from the previous step. Reduce h and repeat a failed corrector; enlarge it only after well-converged steps, within documented bounds. Monitor the mismatch tolerance of 10^{-6} p.u. and the SVG reactive limits at every accepted point. Locate an SVG-limit crossing before continuing, fix Q_{SVG} at the crossed bound, release voltage regulation, rebuild the active equations and tangent, and continue with the updated PQ model. Refine the maximum λ by bracketing the sign change of the tangent component $d\lambda/ds$ through the nose and reducing the step; compare

the refined limit with $\sigma_{\min}(F_x)$. Solver nonconvergence alone is not a demonstrated fold. A limit-induced termination must be reported separately. The 0.95 p.u. voltage criterion is also separate from the fold: the nominal point already violates it in both reported configurations.

5.2. Network and Simulation Parameters

A common per-unit base is adopted at the PCC as

$$S_B = 100MVA, V_B = 20kV \tag{71}$$

The corresponding base impedance is

$$Z_B = V_B^2 \Big/ S_B = \left(20\times10^3\right)^2 \Big/ \left(100\times10^6\right) = 4\Omega \tag{72}$$

For the adopted short-circuit ratio $SCR = 5$, referenced to the 12 MW PV plant,

$$S_{sc} = SCR \cdot P_{PV,rated} = 5\times12 = 60MVA \tag{73}$$

The equivalent grid impedance magnitude referred to the 20 kV PCC is

$$\left|Z_{th}\right| = V_{PCC}^2 \Big/ S_{sc} = \left(20\times10^3\right)^2 \Big/ \left(60\times10^6\right) = 6.667\Omega \tag{74}$$

With $X_{th}/R_{th} = 10$,

$$R_{th} = \left|Z_{th}\right| \Big/ \sqrt{\left(1+10^2\right)} = 0.663\Omega, X_{th} = 10R_{th} = 6.634\Omega \tag{75}$$

Table 6. Main simulation parameters.

Parameter	Symbol	Value	Unit
Power base	S_B	100	MVA
PCC voltage	V_{PCC}	20	kV
PV rated power	P_{PV}, rated	12	MW
Industrial load	S_{I0}	22	MVA
Load power factor	pf_{I0}	0.85	—
Short-circuit ratio	SCR	5	—
Grid X/R ratio	X_{th}/R_{th}	10	—
SVG rating	Q_{SVG}, rated	±6	MVAr
NR tolerance	ε	10^{-6}	—

On the 100 MVA, 20 kV base, the derived upstream equivalent is $R_{th} \approx 0.1658$ p.u. and $X_{th} \approx 1.6584$ p.u. Its magnitude is 1.6667 p.u. SCR and X/R constrain this aggregate equivalent but do not determine the downstream feeder, transformer, or shunt parameters (Table 6).

5.3. Performance Indices and Comparative Assessment

The uncompensated and SVG-compensated configurations are evaluated using the performance indices summarized in Table 7. Voltage regulation is assessed from the minimum bus voltage and maximum voltage deviation, while network

efficiency is quantified from active and reactive losses. Voltage-stability improvement is evaluated from the critical loading factor and the corresponding loading margin.

Table 7. Performance indices.

Performance index	Definition	Assessment
Minimum bus voltage	$V_{\min} = \min_i \lvert V_i \rvert$	Voltage profile
Maximum voltage deviation	$\Delta V_{\max} = \max_i \lvert 1 - \lvert V_i \rvert \rvert$	Voltage regulation
Active-power losses	P_{loss}	Network efficiency
Reactive-power losses	Q_{loss}	Reactive-power transfer
Critical loading factor	$\lambda_{\max}$	Stability boundary
Loading margin	$\Delta P_{\text{margin}} = \lambda_{\max} P_{L0}$	Loadability

The two compensation configurations must use identical network data, slack settings, industrial-load scaling, and PV injections. Only the industrial-bus SVG is enabled or disabled. Voltage-compliance margin and static fold margin are distinct indices; neither reported nominal solution meets $V_{\min} \geq 0.95$ p.u.

6. Results and Discussion

6.1. Base-Case Power-Flow Assessment

The base case is evaluated for $P_{PV} = 12$ MW, $S_L = 22$ MVA, $pf_L = 0.85$, and $Q_{SVG} = 0$. The corresponding industrial demand is $P_L = 18.70$ MW and $Q_L = 11.59$ MVAr. The reduced benchmark yields a minimum voltage of 0.617 p.u. at the industrial bus, indicating a severely stressed operating condition for the adopted $SCR = 5$, as shown in Figure 3.

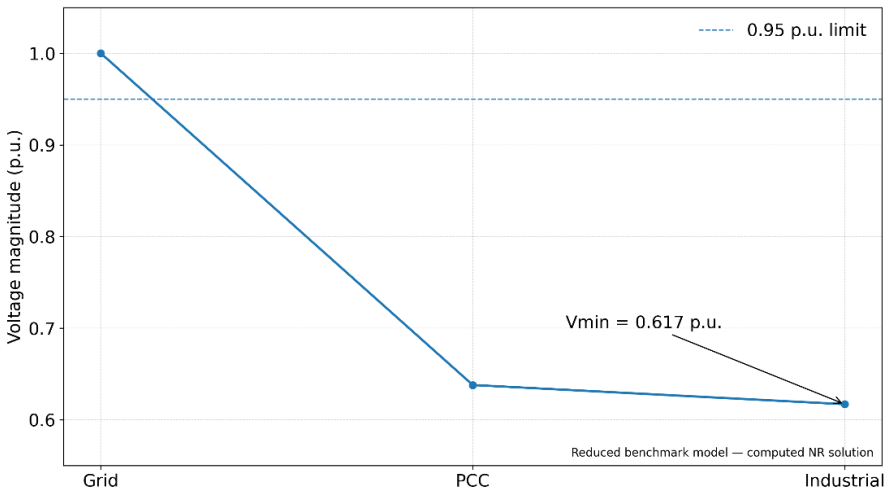


Figure 3. Base-case bus-voltage profile without SVG compensation.

The active-power losses are 0.924 MW in the uncompensated base case. The

industrial bus is therefore retained as the critical bus for the continuation analysis.

6.2. Uncompensated Voltage-Stability Assessment

The industrial demand is progressively increased at constant power factor. The uncompensated P-V trajectory is shown in Figure 4.

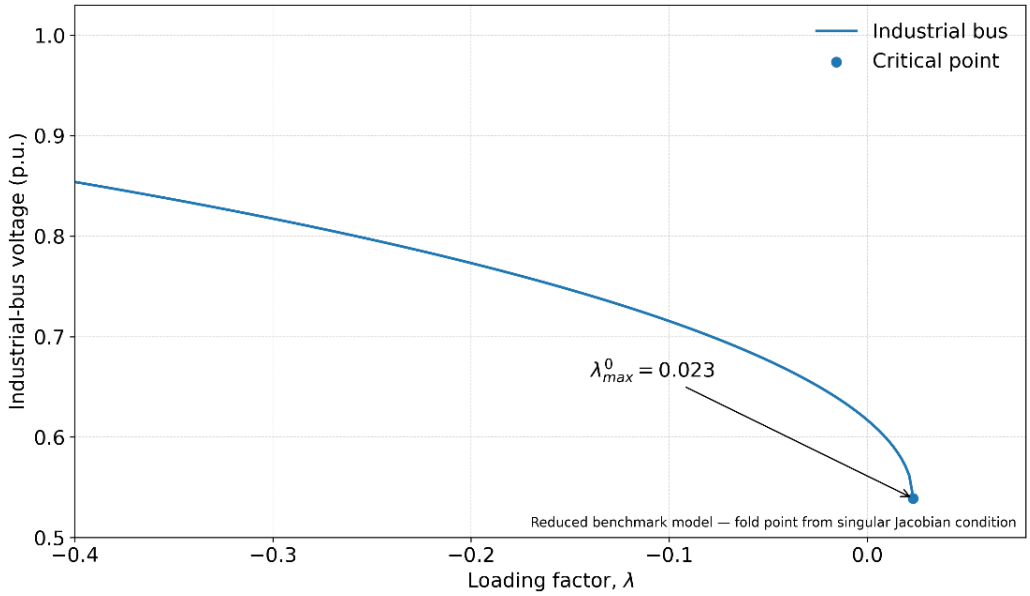


Figure 4. Industrial-bus P-V characteristic without SVG; $\lambda = 0$ denotes 22 MVA nominal demand.

The fold condition is reached at approximately

$$\lambda_{\max}{}^{0} \approx 0.023; P_{L,\max}{}^{0} = 18.70(1+0.023) \approx 19.13MW$$

The reported incremental loading margin is approximately 0.43 MW, or 2.3% of nominal demand. The original 19.11 MW figure is inconsistent with the reported $\lambda_{\max} = 0.023$; 19.13 MW follows from Equation (61). Final values should be calculated from the unrounded continuation export. The listed $\lambda = 0.25$ and 0.50 load cases lie beyond this reported uncompensated limit and must not be presented as feasible solutions on the same branch.

6.3. SVG Compensation Assessment

A 6 MVAr SVG is connected at the critical industrial bus while all other operating parameters remain unchanged. The compensated base-case voltage rises from 0.617 p.u. to 0.855 p.u., as shown in Figure 5.

The reported active-power losses decrease from 0.924 MW to 0.210 MW, while the nominal industrial voltage remains 0.855 p.u., below 0.95 p.u. The SVG nameplate rating does not specify its realized injection. These numerical comparisons remain conditional on verification of the network dataset and control settings.

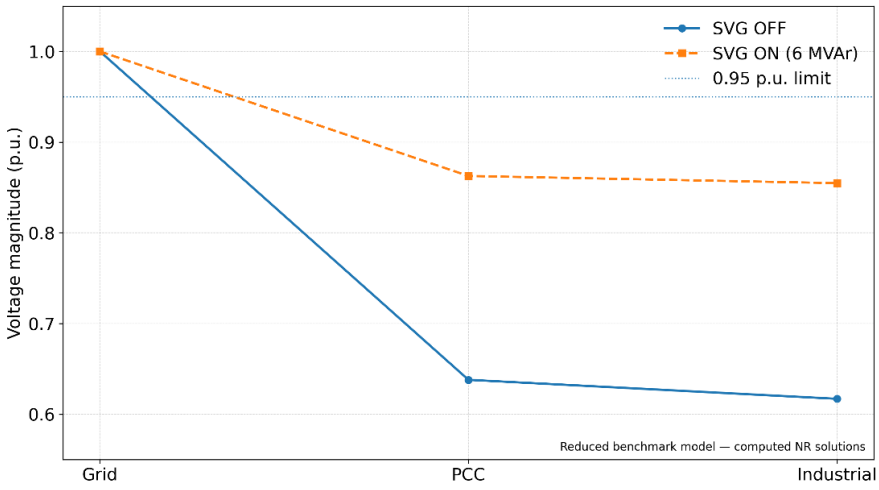


Figure 5. Base-case voltage profiles with and without 6 MVAr SVG compensation.

6.4. Voltage-Stability Margin Enhancement

The continuation analysis is repeated with the 6 MVAr SVG in service. **Figure 6** compares the uncompensated and compensated P-V trajectories.

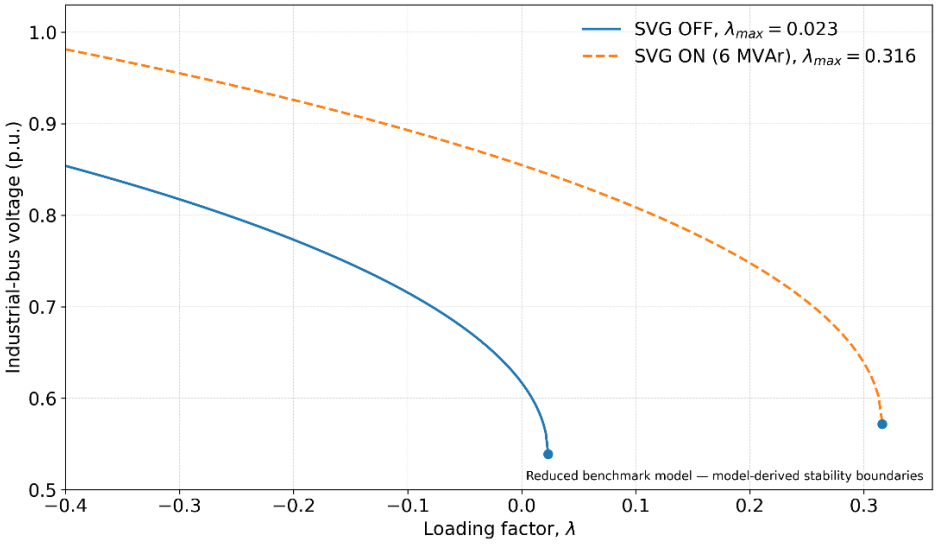


Figure 6. Industrial-bus P-V comparison; the same nominal convention $\lambda = 0$ and industrial-bus SVG location apply to both curves.

The calculated stability boundary shifts from

$$\lambda_{\max}^{0} \approx 0.023 \; to \; \lambda_{\max}^{SVG} \approx 0.316$$

Using Equation (61) with the rounded loading parameters, the maximum industrial active demand increases from 19.13 MW to 24.61 MW. The reported fold margin therefore increases from approximately 0.43 MW to 5.91 MW. This static loadability improvement does not establish compliance with the nominal 0.95 p.u. voltage criterion.

6.5. Comparative Performance and Rating Implication

Table 8. Comparative performance for the reduced benchmark.

Indicator	SVG OFF	SVG ON (6 MVAr)	Assessment
V_{min} (p.u.)	0.617	0.855	Improved; <0.95 p.u.
P_{loss} (MW)	0.924	0.210	Reduced
Q_{loss} (MVAr)	9.875	2.361	Reduced
λ_{max} (increment above nominal)	0.023	0.316	Increased
$P_{L,max}$ (MW)	19.13	24.61	Increased
$\alpha_{max} = 1 + \lambda_{max}$	1.023	1.316	Total load multiplier
ΔP_{margin} (MW)	0.43	5.91	Derived from rounded λ
Actual Q_{SVG} at $\lambda = 0$ (MVAr)	0	Export required	Rating is not injection
Actual Q_{SVG} at λ_{max} (MVAr)	0	Export required	Control regime to confirm

The reported comparison indicates improved voltage support and static loading margin with the initial 6 MVAr SVG rating. A final size cannot be validated until the numerical network and SVG settings are documented and the continuation results reproduced. For the reported compensated limit $\lambda_{max} = 0.316$, the $\lambda = 0.25$ screening point is within the indicated fold range, whereas $\lambda = 0.50$ is outside it; voltage compliance must still be checked independently (Table 8).

$$Q_{SVG,rated} \in \{6,9,12\}\ MVAr$$

The minimum rating satisfying the voltage criterion while preserving the largest practical loading margin should be retained as the final compensation size.

7. Conclusion

This study formulates a static voltage-stability assessment for a 12 MW PV plant and a nominal 22 MVA constant-power industrial load. With $\lambda = 0$ at nominal demand, the reported uncompensated and compensated limits correspond to incremental loading margins of 2.3% and 31.6%. A 6 MVAr SVG at the industrial bus is associated with reported minimum voltages of 0.617 and 0.855 p.u. without and with compensation, respectively; neither nominal point satisfies the 0.95 p.u. criterion. The associated maximum active demands are 19.13 and 24.61 MW when calculated from the reported rounded λ values. Complete network data, actual SVG settings and injections, and a continuation log are required before these numerical conclusions can be regarded as reproducible. The static constant-power model does not establish dynamic industrial-load performance.

Author Contributions

Rodolphe Gomba: Conceptualization, data curation, formal analysis, acquisition funding, survey, methodology, project administration, resources, supervision, val-

idation, visualization and writing: original draft.

Eyandzi Amos Omboua: Software, supervision, validation, visualization, writing—revision and editing.

Conflicts of Interest

The authors declare no conflicts of interest regarding the publication of this paper.

References

[1] Saleem, M.I., Saha, S., Izhar, U. and Ang, L. (2024) Stability Assessment of Inverter-based Renewable Energy Sources Integrated to Weak Grids. *IET Energy Systems Integration*, **6**, 525-544. https://doi.org/10.1049/esi2.12151

[2] Sanni, S.O., Abdullateef, A.I., Mohammed, O.O., Aman, M.N., Raji, A.K. and Fajuke, I.D. (2024) Investigating the Impact of Solar PV and Wind Energy Systems on the Strength of a Longitudinal Power Grid. *e-Prime—Advances in Electrical Engineering, Electronics and Energy*, **8**, Article 100593. https://doi.org/10.1016/j.prime.2024.100593

[3] Zhang, Q., Hu, Q., Sun, S., Mei, D., Liu, S. and Liu, X. (2023) Voltage and Frequency Instability in Large PV Systems Connected to Weak Power Grid. *Frontiers in Energy Research*, **11**, Article 1210514. https://doi.org/10.3389/fenrg.2023.1210514

[4] Lei, P. and Zhao, J. (2024) The Analysis of the Threshold Value of the Complex Short-Circuit Ratio Index and Its Significance in the Context of Static Voltage Stability. *Frontiers in Energy Research*, **12**, Article 1413910. https://doi.org/10.3389/fenrg.2024.1413910

[5] Yu, L., Xu, S., Sun, H., Zhao, B., Wu, G. and Zhou, X. (2024) Multiple Renewable Short-Circuit Ratio for Assessing Weak System Strength with Inverter-Based Resources. *CSEE Journal of Power and Energy Systems*, **10**, 2271-2282.

[6] Miyazaki, M., Aoki, M. and Nakamura, Y. (2025) Voltage Stability Estimation Considering Variability in Reactive Power Reserves Using Regression Trees. *Energies*, **18**, Article No. 1260. https://doi.org/10.3390/en18051260

[7] Yenealem, M.G. (2025) Voltage Stability Assessment and Improvement of Ethiopian 230 kV Wind-Integrated Grid Using SVC and Continuation Power Flow in PSAT. *Scientific Reports*, **15**, Article No. 31946. https://doi.org/10.1038/s41598-025-13206-w

[8] Adetona, S., Balogun, A., Esenwa, E., Olajube, A., Awelewa, A. and Okafor, F. (2024) A Model Predictive Control-Based STATCOM for Weak Grid Voltage Enhancement. *Engineering and Technology Journal*, **42**, 1138-1154. https://doi.org/10.30684/etj.2024.149900.1752

[9] Cao, J., Liu, M., Ma, Q., Fan, J., Song, D., Zhou, X., *et al.* (2025) Assessment of Grid-Tied Renewable Energy Systems' Voltage Support Capability under Various Reactive Power Compensation Devices. *Energies*, **18**, Article No. 3880. https://doi.org/10.3390/en18143880

[10] Zhang, S., Chen, Y., Li, Q., Xie, Z., Fu, Y. and Wu, W. (2025) Quantitative Stability Analysis of STATCOM in Voltage Control Mode and Enhanced Control Method Based on Voltage Feedforward. *International Journal of Electrical Power & Energy Systems*, **171**, Article 110975. https://doi.org/10.1016/j.ijepes.2025.110975

[11] Liu, J., Wang, L., Jiao, T., Yang, W., Xu, R., Wu, K., *et al.* (2024) Multi-Period Voltage Stability-Constrained Optimal Power Flow with Uncertainties. *Applied Energy*, **369**, Article 123522. https://doi.org/10.1016/j.apenergy.2024.123522

[12] Kim, H., Woo, H., Yoon, Y., Kim, H., Kim, Y.J., Kang, M., *et al.* (2024) An Enhanced Continuation Power Flow Method Using Hybrid Parameterization. *Sustainability*, **16**, Article 7595. https://doi.org/10.3390/su16177595

[13] Wang, T., Wang, S., Ma, S., Guo, J. and Zhou, X. (2024) An Extended Continuation Power Flow Method for Static Voltage Stability Assessment of Renewable Power Generation-Penetrated Power Systems. *IEEE Transactions on Circuits and Systems II: Express Briefs*, **71**, 892-896. https://doi.org/10.1109/tcsii.2022.3209335

[14] Suresh, A., Hasan, M.S., Kamalasadan, S. and Paudyal, S. (2025) A Distributed Energy Resources Integrated Transmission and Distribution Continuation Power Flow Model with Sequence Component Approach. *IEEE Transactions on Industry Applications*, **61**, 5637-5648. https://doi.org/10.1109/tia.2025.3544982

[15] Al-Majali, B.H. and Zobaa, A.F. (2025) A Novel Optimal Allocation of STATCOM to Enhance Voltage Stability in Power Networks. *Ain Shams Engineering Journal*, **15**, Article 102658. https://doi.org/10.1016/j.asej.2024.102658